Article ID: 1003－6326(2004)03－0505－05

Influence of heat treatment regimes on microstructures and fracture characteristics of 7055Al alloy containing Ag①

LI Hai(李 海), ZHENG Zi-qiao(郑子樵), WANG Zhi-xiu(王芝秀)
(School of Materials Science and Engineering, Central South University, Changsha 410083, China)

Abstract: Tensile properties, fracture characteristics and microstructures of 7055 aluminum-based alloy containing Ag after T6, T73 and RRA treatment were investigated. The results show that RRA treatment retains strength of 7055-T6 with higher electrical conductivity close to that of 7055-T73 alloy, but its elongation decreases greatly. SEM fractographs reveal that intergranular cracking and shear-type transgranular cracking are both presented on the fracture appearance of 7055-T6 specimen. After T73 treatment, the fractographs mainly consist of dimple-type transgranular cracking with minor intergranular cracking. For 7055-RRA specimen, intergranular cracking dominates with minor dimples on the fracture surface. The type and size of precipitates, width of grain boundary and the ability of precipitates to impede dislocation motion vary with heat treatment regimes. Three frature models were built on the basis of microstructural analyses.

Key words: 7055Al alloy; heat treatment; fracture characteristic; intergranular cracking; transgranular cracking
CLC number: TG 146 **Document code:** A

1 INTRODUCTION

Al-Zn-Mg-Cu aluminum-based alloys, which can give the highest ageing strength among aluminum alloy series, have extensive applications in aerospace industry. But in T6 condition, the alloys is susceptible to stress corrosion cracking (SCC). Conventional over-ageing treatment, for example, T73, can improve stress corrosion resistance (SCR), but with 10%－20% loss of strength. Recently developed retrogression and reageing(RRA) treatment can also enhance SCR without loss of strength, and receives extensive attention[1-9]. However, RRA treatment often causes decrease in ductility, which is more serious in the higher Zn content alloys[5-9].

In the present work the tensile fracture appearance of 7055Al alloy containing minor Ag in T6, T73, RRA tempers was investigated, and the corresponding fracture models on the basis of the analyses of TEM microstructures were established.

2 EXPERIMENTAL

The experimental materials were 7055Al alloy sheets cold rolled to 2 mm-thick, and the chemical compositions was listed in Table 1. Specimens with a gauge length of 90 mm and a gauge width of 18 mm were machined from the sheets. Solution treatment was carried out at 470 ℃ for 1 h followed by water quenching. Three heat treatment regimes were used: 1) T6, 120 ℃, 24 h; 2) RRA, T6+ 180 ℃, 45 min+ T6; and 3) T73, 108 ℃, 8 h+ 160 ℃, 18 h. Electrical conductivity was tested using double bridge method. After the measurement of the electrical conductivity, tensile specimens with a gauge size of 34 mm(length) × 8 mm(width) were machined from the electrical conductivity specimens and tested on CSS machine. Tensile fractographs were observed on KYKY-2800 scanning electron microscopy. TEM films were prepared from the gauges and grips of the tensile specimens respectively. Microstructures were observed on H-800 transmission electron microscope.

Table 1 Chemical compositions of studied 7055Al alloy(mass fraction, %)

Zn	Mg	Cu	Zr	Fe	Si	Ag	Al
7.36	2.04	2.29	0.12	0.1	0.06	0.5	Bal.

3 RESULTS

3.1 Mechanical properties and electrical conductivity

Tensile properties and electrical conductivity of 7055Al alloy under three ageing conditions are listed in Table 2. The data in Table 2 suggested that enhanced strength and ductility in 7055-T6 alloy were received, but with reduced electrical conductivity. In

① **Foundation item:** Project(G1999064900-9) supported by the National Key Fundamental Research and Development Program of China
Received date: 2003－08－27; **Accepted date:** 2004－01－10
Correspondence: LI Hai, PhD candidate; Tel: +86-731-8832422; E-mail: lehigh_73@163.com

comparison with 7055-T6 alloy, strength of 7055-RRA alloy remains unchanged and electrical conductivity increases. However, the ductility of 7055-RRA alloy decreases markedly. Though the ductility and electrical conductivity of the alloy increases compared with 7055-T6 alloy, the strength of 7055-T73 alloy reduces greatly. The measurement of the electrical conductivity is often used as a criterion of the resistance of Al-Zn-Mg-Cu alloy to SCC in practical applications. Usually, 38% (IACS) is accepted as the lower limit of Al-Zn-Mg-Cu alloys unsusceptible to SCC[9]. From the data listed in Table 2, 7055-RRA and T73 alloy are not prone to SCC, but 7055-T6 alloy has higher susceptibility to SCC.

Table 2 Tensile properties and electrical conductivity of 7055Al alloys under three ageing conditions

Heat treatment	Tensile strength, σ_b/MPa	Yield strength, $\sigma_{0.2}$/MPa	Elongation, δ/%	Electrical conductivity/% (IACS)
T6	635.1	612.4	8.7	32.4
RRA	635.6	623.7	5.4	38.1
T73	526.4	498.6	11.2	42.1

3.2 SEM fractography

SEM fractographs of 7055-T6, T73 and RRA alloys are given in Fig. 1. Fig. 1(b), (d) and (f) show high magnification observation of the square parts in Fig. 1 (a), (c) and (e), respectively. Both transgranular shearing ledges and secondary cracks were distributed on the fracture surfaces of 7055-T6 alloy (Fig. 1(a) and (b)). 7055-T73 alloy has typical dimple-type fracture characteristics and broken second phase particles are found within the dimples. Secondary cracks distributed along grain and subgrain boundaries reduce markedly (Fig. 1(c) and (d)), which suggestes that the ductility of 7055-T73 alloy has been improved. The rock-type fractography of 7055- RRA alloy with small dimples on the grain boundaries reveals that the cracks propagate along grain boundaries (Fig. 1(e) and (f)). The above analyses of the fractography show that, under the three conditions of 7055-T6, T73 and RRA, both transgranular and intergranular fracture characteristics simultaneously appeare on the tensile fractography. However, the proportion of transgranular cracking

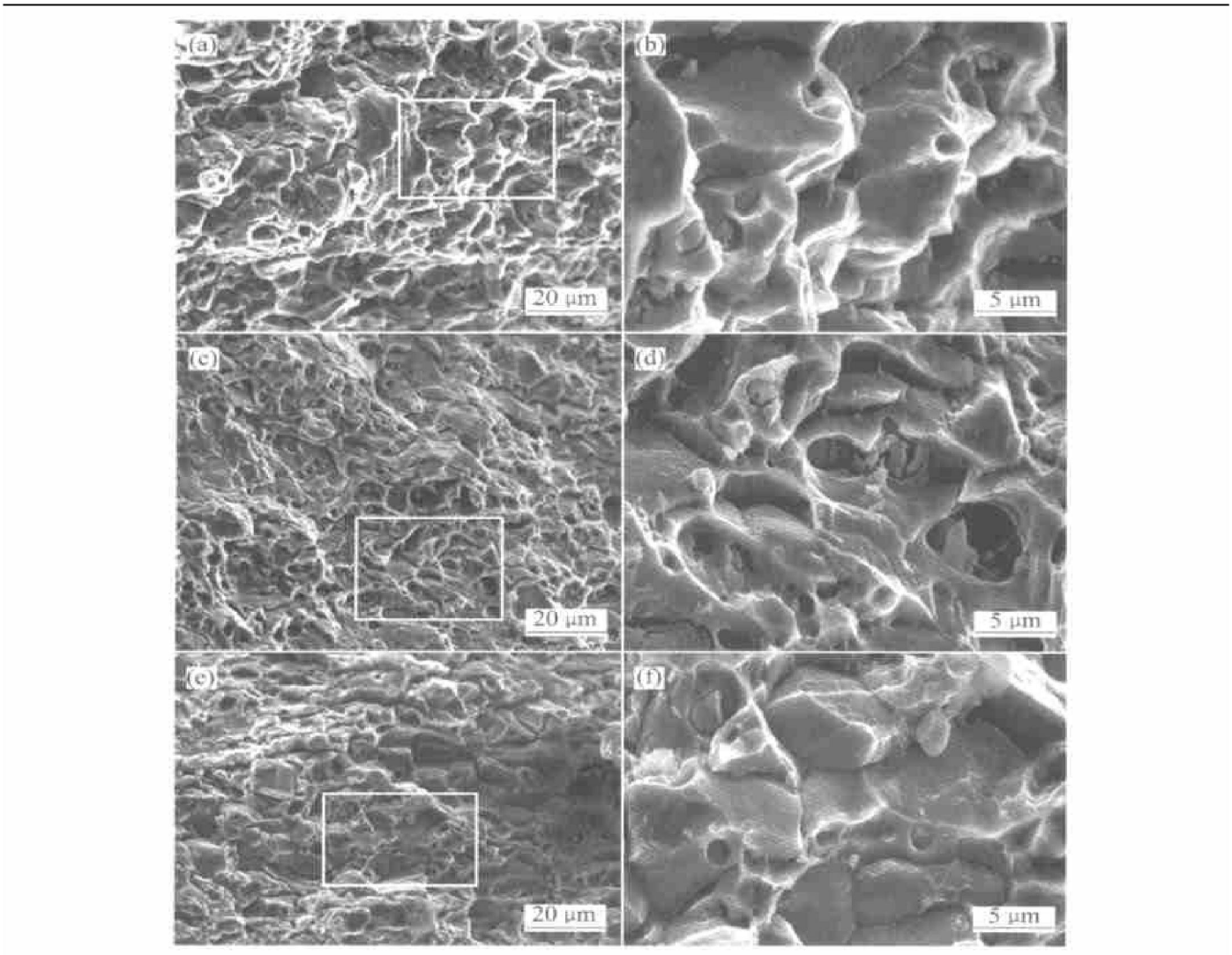

Fig. 1 TEM fractography in 7055-T6, T73 and RRA.
(a) and (b) —T6; (c) and (d) —T73; (e) and (f) —RRA

varies with heat treatment regimes and the corresponding elongation of the alloy alters, that is, $\delta_{T73} > \delta_{T6} > \delta_{RRA}$ (Table 2).

3.3 TEM microstructures

TEM microstructures of 7055-T6, RRA and T73 alloy are shown in Fig. 2. Figs. 2(a), (c) and (e) present microstructures in the grips of tensile specimen, revealing non-deformed microstructures. Figs. 2(b), (d) and (f) suggest deformed microstructures within the gauge of the tensile specimen. The precipitates in 7055-T6 alloy are finely and uniformly dispersed inside the grains. Grain boundary precipitates are coarse and continuously dispersed, and the width of grain boundary is very narrow. After tensile deformation, the parallel lath-type structures occurred inside the grains, as shown in Fig. 2(b). After RRA treatment, both matrix precipitates and grain boundary precipitates further coarsened, suggesting that the precipitates grew and corresponding grain boundary widened (Fig. 2(c)). The parallel lath-type structures still remain inside the matrix (Fig. 2(d)). After T73 treatment, the precipitates within the grains and at grain boundaries grow and the width of grain boundary further increases (Fig. 2(e)). Dislocations distribute homogeneously in the deformed matrix, and there are no lath-type structures (Fig. 2(f)).

TEM microstructures exhibiting dislocation motion are shown in Fig. 3. From Fig. 3(a), regular sliding bands with included angle of 60° shows

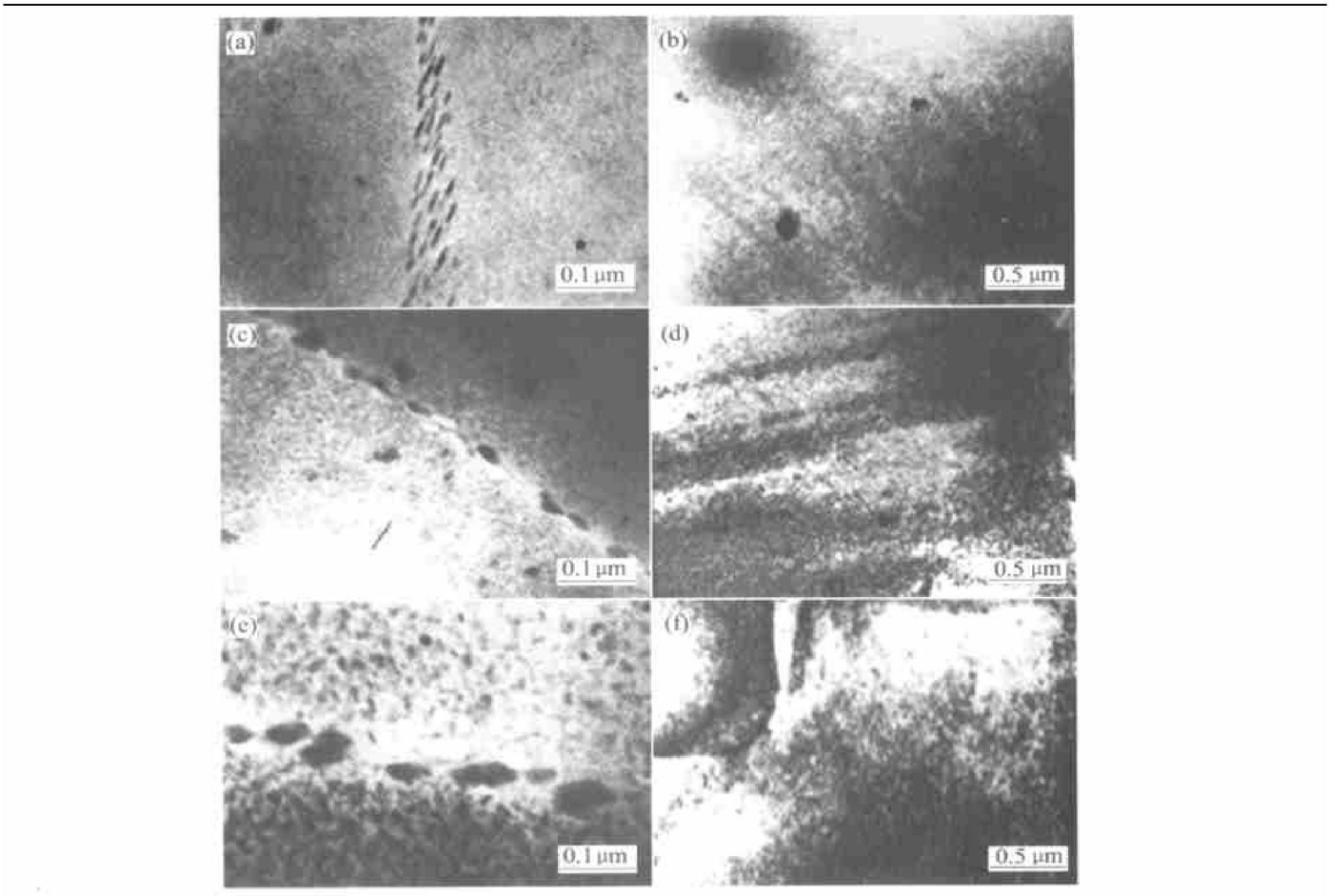

Fig. 2 TEM characteristics of precipitates, dislocations and grain boundary after different treatments
(a) and (b) —T6; (c) and (d) —RRA; (e) and (f) —T73

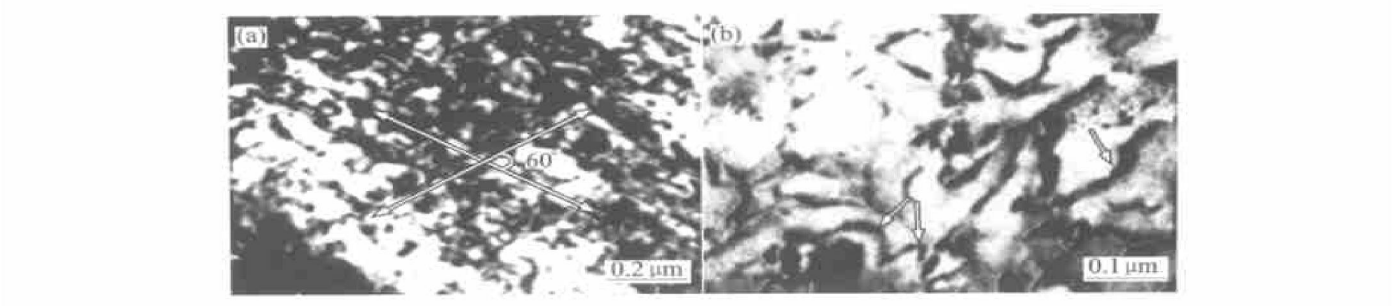

Fig. 3 Disloction motion
(a) —T6; (b) —T73

that disloctoins slide repeatedly along a lattice direction on a lattice plane. As for FCC Al-Zn-Mg-Cu alloys, sliding planes and sliding directions are close-packed {111} and ⟨110⟩ respectively. The main strengthening phases, GP zones, η′ ($MgZn_2$) and η ($MgZn_2$) of Al-Zn-Mg-Cu alloys are also precipitated on {111} planes. Therefore, the precipitates in the grains are sheared by sliding dislocations. No regular sliding bands are seen in 7055-T73 alloy and dislocations pass through the matrix by Orowan mechanims, which suggests homogeneous deformation in 7055-T73 alloy, as shown by arrow in Fig. 3(b).

4 DISCUSSION

4.1 Microstructures

It is known that, the matrix precipitates of Al-Zn-Mg-Cu-T6 alloy mainly consist of coherent GP zones riched in Zn and Mg elements and small amount of semi-coherent η′ ($MgZn_2$) phases. Coarse and non-coherent η ($MgZn_2$) phases distribute continuously on grain boundaries[10]. Grain boundary is very narrow (Fig. 2(a)). Overageing treatment, such as T73, promotes the precipitation of coarse and non-coherent η phases inside the matrix[10]. The strength of 7055-T73 alloy decreases due to the increase of the spacing between η particles and the growth of their sizes. The width of grain boundary increases and at grain boundary η phases become coarser and discontinuous (Fig. 2(e)), which causes 7055-T73 alloy unsusceptible to SCC.

As for 7055-RRA alloy, the solvus of GP zones shifts from 130 – 140 ℃ to almost 200 ℃ as a result of the minor addition of Ag[11], therefore, a majority of GP zones do not reverse, but transform into η′ phases during 180 ℃ retrogression. Small part of GP zones whose sizes were smaller than the critical value can reverse and appear in the form of solute atoms. The η′ precipitates do not reverse during the first T6 treatment, because the solvus of η′ is beyond 250 ℃. Therefore, a part of η′ phases remain and another part of η′ phases maybe transform into η phase. In the course of reageing, the solute atoms which form during retrogression precipitate again in the form of GP zone and η′ phase. The majority of η′ phases after retrogression remain and the remainder transforms into η phases. As a result, the major strengthening phase in RRA alloy consists mainly of η′ phases, partial GP zones and η phases (Fig. 2(c)). On one hand, the precipitation of η phases lowers the strength of the alloy; On the other hand, the volume fraction of η′ phases increases and the strengthening potential of η′ phases is greater than that of GP zones and η phases, so it can compensate the strength loss as a result of the precipitation of η phases[12, 13]. Therefore, RRA treatment can receive the strength similar to that of 7055-T6 alloy. η phases at grain boundary do not reverse during retrogression, on the contrary, the width of grain boundary and the spacing among η phases at grain boundaries increases, leading to SCR of 7055-RRA alloy close to that of T73 treatment.

4.2 Fracture modelling

As mentioned above, the types and sizes of strengthening precipitates and width of grain boundary vary with heat treat regimes and correspondingly the properties of the alloys change. After T6 treatment, matrix precipitates mainly consist of GP zones and partial η′ phases. The two precipitates are coherent with the matrix to some degree and can be sheared off by dislocations during tensile deformation[14]. When dislocations move along a lattice direction on a lattice plane, the precipitates are sheared off and the volume of the precipitates decreases, as shown in Fig. 3(a). Therefore, the resistance to dislocation motion reduces, which leads to repeated motion of dislocation on the lattice plane. As a result, the localized deformation bands occur, as shown in Figs. 2(b) and (d). This is in agreement with the results in Ref. [15]. The localized deformation bands intersect with grain boundaries and form grain boundary steps. Because of very narrow grain boundary, the strength difference between the matrix and grain boundary is negligible. The repeated motion of dislocations form piles-up near grain boundaries. Stress concentration formed by dislocation piles-up can produce cracks initiation along grain boundaries and steps simultaneously, avoiding the simple cracking along grain boundaries. Therefore, the ductility of 7055-T6 increases. Cracking along steps on grain boundaries causes shear-type transgranular fracture, as shown in Figs. 1(a) and (b).

After T73 treatment, the coarsening of η phases at grain boundaries and the widening of grain boundary decrease the strength near grain boundary. However, the precipitation of coarse η phases inside the matrix also lowers matrix strength. Strength difference between matrix and grain boundary is also small, leading to relatively homogeneous deformaion within the matrix and grain boundary. Furthermore, when sliding dislocations encounter non-coherent η phases within the matrix, dislocations can not shear η phases, but piled up before η phases. When stress concentration exceeds the resistance of η phases, piled-up dislocations can continue to move (Fig. 3(b)). The dislocation sliding modes can lower the extent of stress concentration near grain boundaries and enhance stress within grains. The stress causes crack initiation at the interface between coarse secondary phases and the matrix, so the dimple-type transgranular cracking occurs and the elongation of 7055-T73 alloy is enhanced.

The strengthening precipitates mainly consist of η′ phases, partial GP zones and η phase after RRA treatment. Due to the presence of shearable GP zones and η′ phases, repeated sliding of dislocations still produce piles-up at the grain boundaries, and cause stress concentration near grain boundaries. Meanwhile, after RRA treatment matrix strength maintains and grain boundary strength decreases. Strength difference between matrix and grain boundary becomes larger, which causes the localized deformation near grain boundaries under the combined roles of applied stress and stress concentration produced by dislocation piles-up. Correspondingly, the elongation of 7055-RRA reduces. When deformation is localized near grain boundaries, microcracks initiate at the interface between grains and coarse η phases at grain boundary, producing grain boundary dimples, as shown in Figs. 1(e) and (f).

On the basis of the above analyses, three fracture models can be established, as shown in Fig. 4.

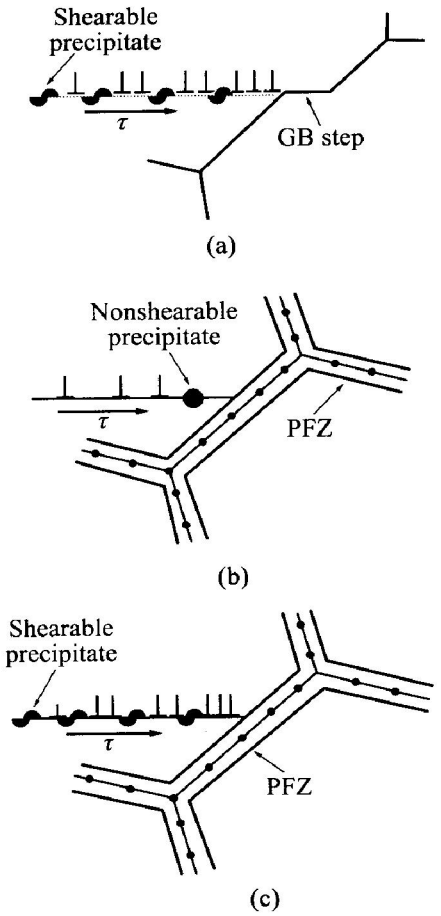

Fig. 4 Schematic illustration of deformation and fracture model of 7075Al alloy under different treatments
(a) —T6; (b) —T73; (c) —RRA

REFERENCES

[1] Cina B. Reducing the Susceptibility of Alloy, Particular Aluminum Alloys to Stress Corrosion Cracking[P]. US 3856584, 1974.

[2] Rajan K, Wallace W, Beddoes J C. Microstructural study of a high-strength stress-corrosion resistant 7075 aluminum alloy[J]. J Mat Sci, 1982, 17: 2817-2824.

[3] Danh N C, Rajan K, Wallace W. A TEM study of microstructural changes during retrogression and reaging in 7075 aluminum[J]. Metal Trans, 1983, 14A: 1843-1850.

[4] Park J K, Ardell A J. Effect of retrogression and reaging treatments on the microstructure of Al 7075-T651[J]. Metall Trans, 1984 15A: 1531-1543.

[5] ZHENG Zi-qiao, LI Hong-ying, MO Zhi-ming. Retrogression and re-aging treatment of a 7055 type aluminium alloy[J]. The Chinese Journal of Nonferrous Metals, 2001, 11(5): 771-776. (in Chinese)

[6] Osaki S, Itoh D, Nakai M. SCC properties of 7050 series aluminum alloys in T6 and RRA tempers[J]. JILM, 2001, 51(4): 222-227.

[7] WU Yi-Lei, (Sam) fores F H, Li Chewnggong, et al. Microalloying of Sc, Ni, and Ce in an advanced Al-Zn-Mg-Cu alloy[J]. Metal Mater Trans, 1999, 30A(4): 1017-1024.

[8] Lee C W, Chung Y H, Cho K K, et al. The effect of silver addition on 7055 Al alloy[J]. Materials and Design, 1997, 18(4/6): 327-332.

[9] Andrzej G, Malgorzata W, Wojciech W. DTA investigation of the retrogression and re-ageing in some AlZnMgCu alloys[J]. Thermochimica Acta, 1997, 303: 197-202.

[10] Loffer H, Kovacs I, Lendvai J. Decomposition processes in Al-Zn-Mg alloys[J]. J Mat Sci, 1983, 18: 2215-2240.

[11] Viets J T, Sargant K R, Polmear I J. The influence of small additions of silver on the ageing aluminium alloys: further observations on Al-Zn-Mg alloys[J]. JIM, 1963-1964, 92: 327-334.

[12] HUA Ming-jian, LI Chun-zhi, WANG Hong-jian. Effect of microstructures on the yield strength and SCR of 7075 aluminium alloy[J]. Acta Metall Sinica, 1988, 24(1): 41-46. (in Chinese)

[13] SONG Ren-guo, ZHANG Bao-jin, ZENG Mei-guang. Investigation of stress corrosion susceptibility for 7175 aluminium alloy double peak aged[J]. Trans of Metal Heat Treatment, 1996, 17(2): 51-54. (in Chinese)

[14] Kuramoto S, Itoh G, Kanno M. Intergranular fracture in some precipitation-hardened aluminum alloys at low temperatures[J]. Met Mater Trans, 1996, 27A: 3081-3088.

[15] Srivatsan T S, Anand S, Veeraghavan D, et al. The tensile response and fracture behavior of an Al-Zn-M-Cu alloy: influence of temperature[J]. J Materials Engineering and Performance, 1997, 6(3): 349-358.

(Edited by YANG Bing)